Development of a Synchronization Method for Fluid-Thermal Study of Hypersonic Flow

Shen Ennan, Lu Zhiliang, Zhou Di, Guo Tongqing*

College of Aerospace Engineering, Nanjing University of Aeronautics and Astronautics, Nanjing 210016, P. R. China

(Received 2 November 2017; revised 16 January 2018; accepted 20 January 2018)

Abstract: A synchronization method is developed for the fluid-thermal study of hypersonic flow. Different from conventional loosely/tightly coupled methods which separately deal with the flow field and the structure temperature field, the presented method expresses the governing equations in a unified framework so that the two fields can be calculated simultaneously. For efficiently solving the unified equations, the finite volume method together with the dual-time stepping approach is employed. Like in the flow field, the local time step is also used in the temperature field, which is determined from thermal conductivity spectral radii. In order to treat the fluid-structure interface more conveniently, an expanded virtual boundary is introduced. For validation, several fluid-thermal hypersonic flow problems are simulated. The computed results are compared with those obtained from the coupled methods and the experiment. In the continuous heating problems, the stagnation temperatures predicted by both the coupled and synchronization methods are in good agreements with the experimental data. In the unsteady flow-thermal hypersonic flows, the stagnation heat fluxes predicted by the presented method and tightly coupled method are basically the same, which agree better with the experimental data than those predicted by the loosely coupled method. In terms of prediction of the stagnation temperature, the synchronization method shows better accuracy than the tightly coupled method.

Key words: hypersonic flow; aerothermal; synchronization method; expanded virtual boundary; conductivity spectral radii

CLC number: O551.3 **Document code**: A **Article ID**: 1005-1120(2018)06-0973-13

Nomenclature

Φ	Variables at cell center
$q/(\mathrm{kW \cdot m^{-2}})$	Rate of heating
$k/(\mathrm{W \cdot (m \cdot K)^{-1}})$	Thermal conductivity
T/K	Temperature
p/Pa	Pressure
$\boldsymbol{n}$	Unit normal vector
$\rho(\mathrm{kg \cdot m^{-3}})$	Density
$C/(\mathrm{J \cdot (kg \cdot K)^{-1}})$	Specific heat
t/s	Time
E	Total energy
$u, v, w/(\mathrm{m \cdot s^{-1}})$	Flow velocity components
γ	1.4, ratio of specific heat of ideal gas
μ	Coefficient of viscosity
P	Prandtl number
C_p	Constant-pressure specific heat in fluid part
σ	CFL number
h	Enthalpy
ρ_0	Density at sea level, set as $1.225\ \mathrm{kg/m^3}$
R_N/m	Stagnation radius
V_c	Set as 7 900 m/s
$h_{300\ \mathrm{K}}$	Enthalpy at 300 K
Subscripts	
s	Solid part
f	Fluid part
L	Laminar flow

* Corresponding author, E-mail address: luzl@nuaa.edu.cn.

How to cite this article: Shen Ennan, Lu Zhiliang, Zhou Di, et al. Development of a synchronization method for fluid-thermal study of hypersonic flow[J]. Trans. Nanjing Univ. Aero. Astro., 2018, 35(6): 973-985.
http://dx.doi.org/10.16356/j.1005-1120.2018.06.973

T Turbulent flow
v Viscous flux
c Convective flux
w Interface between solid and fluid parts
∞ Free-stream parameters
st Stagnation behind the normal shock
wst Stagnation point at wall

0 Introduction

In the research and development of hypersonic vehicles, aerodynamic heating is a major difficulty that needs to be overcome. The transient structural temperature field of a hypersonic vehicle requires accurate computation. In recent years, some coupled methods have been developed to simulate these structure-aerodynamic heating (i. e., flow-thermal) problems. These methods can be classified into two types, namely tightly coupled methods and loosely coupled methods. If a single interface iteration (coupling iteration) is performed at each time step (or stage of an implicit Runge-Kutta scheme), the algorithm is referred to as a loosely coupled method, and otherwise it is referred to as a tightly coupled method[1]. Another way to distinguish them is as follows. Loosely coupled methods presume that the time taken for the flow field to reach equilibrium can be neglected when comparing characteristic time step for heat conduction in the structure; tightly coupled methods presume that the flow field and the heat conduction in the structure should be uniformly solved by a smaller characteristic time step determined by the flow field[2]. Regardless of how these methods are distinguished, most researchers used the exchanging flow field and the structural temperature field boundary conditions to solve the coupling problem when simulating the structural temperature field and the flow field separately[3-9]. Geng et al.[10] proposed an integrated numerical method without iterative coupling of these two fields, which was similar to loosely coupled methods. The flow and heat conduction were described in unified equations. To eliminate huge differences in characteristic time steps between fluid and solid, the flow field was kept "frozen" until the structural surface temperature changed by a certain magnitude.

Most studies on the use of both loosely and tightly coupled methods showed that the former remedies the low computational efficiency of the latter, premised on ensuring the accuracy of the computation[2,7-9]. By using these methods, the information of the two fields needs to be exchanged at the interface, and when one field is being computed, the other is usually kept "frozen". However, this situation is non-physical because both the flow field and the structural temperature field are changing simultaneously, and thus the solution accuracy may be reduced. In addition, the determination of the coupling time step is critical. A very small time step may increase the computational efforts while a very large value may lead to numerical errors. Duchaine et al.[11] proposed a direct coupling method of the fluid/solid domains in a large system of simultaneous equations that is handled by a "monolithic" solver, called parallel coupling strategy (PCS), and has been tested to deal with a fully non-stationary coupled problem with synchronization in physical time. There are still existing exchanges between fluid solver and solid solver.

To overcome these drawbacks and to satisfy engineering requirements in precision as well, a synchronization method to simulate both flow field and structural temperature field for hypersonic vehicles is developed. An expanded virtual boundary is applied at the interface between fluid and solid components. The local time step required for computations involving the solid component is determined from thermal conductivity spectral radii, which is similar to the viscous spectral radii of the fluid. The whole field then remains synchronized in the time domain. The numerical results of the developed synchronization method are compared with those of both loosely and tightly coupled methods and from experiment.

In what follows, we first describe the governing equations for the loosely/tightly coupled systems, and the numerical method in the gas do-

main, the solid domain and at the interface(Section2). In Section3, we present the synchronization method based on expanded virtual boundary and the thermal conductivity spectral radii. In the final part of the paper (Section4), the numerical results of the synchronization method are compared with those obtained from the loosely/tightly coupled methods, and experiment data.

1 Loosely/Tightly Coupled Methods

Traditional coupled methods include both tightly and loosely coupled methods, both of which contain a flow field solver and a thermal conduction solver that work independently but exchange information at the boundary. Since response of flow field is much faster than that of heat conduction, the steady-flow Navier-Stokes (NS) equations are used in loosely coupled methods and the time step is determined from the characteristics of the heat conduction, which differs from that for tightly coupled methods.

1.1 Flow field solver

Consider the three-dimensional NS equation described in the Cartesian coordinate system

$$\frac{\partial \boldsymbol{W}}{\partial t}+\frac{\partial \boldsymbol{f}}{\partial x}+\frac{\partial \boldsymbol{g}}{\partial y}+\frac{\partial \boldsymbol{q}}{\partial z}=\left(\frac{\partial \boldsymbol{R}}{\partial x}+\frac{\partial \boldsymbol{S}}{\partial y}+\frac{\partial \boldsymbol{T}}{\partial z}\right) \quad (1)$$

where $\boldsymbol{W}$ represents the conservative variable, $\boldsymbol{f}$, $\boldsymbol{g}$, $\boldsymbol{q}$ represent the convective flux vectors, and $\boldsymbol{R}$, $\boldsymbol{S}$, $\boldsymbol{T}$ the viscous flux vectors.

In the computation of hypersonic flows, the "advection upstream splitting method" (AUSM +) format has many clear and well-known advantages, such as positive pressure retention, good stability, and high resolution. Viscous fluxes are discretized by the cell central scheme. To improve the accuracy of the calculation, the third-order "monotonic upstream-centered scheme for conservation laws" (MUSCL) interpolation method is applied. As the flow field contains strong gradients, the limiter is required to suppress any numerical oscillation. The MUSCL interpolation method involves

$$\begin{aligned}\Phi^{L}_{i+\frac{1}{2},j}&=\Phi_{i,j}+\\&\frac{\mu_i}{4}\left[(1+\mu\bar{\omega})\Delta_{+}\Phi+(1-\mu\bar{\omega})\Delta_{-}\Phi\right]_i\\\Phi^{R}_{i+\frac{1}{2},j}&=\Phi_{i+1,j}-\\&\frac{\mu_{i+1}}{4}\left[(1+\mu\bar{\omega})\Delta_{-}\Phi+(1-\mu\bar{\omega})\Delta_{+}\Phi\right]_{i+1}\end{aligned} \quad (2)$$

By setting $\bar{\omega}=1/3$ in Eq. (2), the third-order upwind-biased scheme is obtained. Δ_{+} and Δ_{-} represent the forward and the backward differences, respectively. The van Albada limiter μ is given by

$$\mu=\frac{2\Delta_{+}\cdot\Delta_{-}+\varepsilon}{\Delta_{+}^{2}+\Delta_{-}^{2}+\varepsilon} \quad (3)$$

where ε is set to 10^{-6}.

For loosely coupled methods, the steady-flow NS equation is implemented in the flow field solver, and the implicit lower-upper symmetric Gauss-Seidel (LU-SGS) scheme is applied to temporal discretization; For tightly coupled methods, the unsteady-flow NS equation is applied to the flow field solver, and the dual time stepping method is applied to temporal discretization. The far field has non-reflecting boundary conditions imposed, and no-slip wall conditions are imposed at the interface between the solid and viscous flow. The conditions imposed for the heat flux at the isothermal boundary and the pressure gradient at the solid surface are

$$q=k\cdot\frac{\partial T}{\partial \boldsymbol{n}} \quad (4)$$

$$\frac{\partial p}{\partial \boldsymbol{n}}=0 \quad (5)$$

1.2 Thermal conduction solver

Assuming no heat sources, the heat equation is given by

$$\rho_s C_s\frac{\partial T}{\partial t}=k_s\left(\frac{\partial^2 T}{\partial x^2}+\frac{\partial^2 T}{\partial y^2}+\frac{\partial^2 T}{\partial z^2}\right) \quad (6)$$

The integral form of the thermal conduction control equation is then

$$\begin{aligned}&\int_{\Omega}\rho_s C_s\frac{\partial T}{\partial t}\mathrm{d}\Omega=\\&\int_{\Omega}k_s\left[\frac{\partial}{\partial x}\left(\frac{\partial T}{\partial x}\right)+\frac{\partial}{\partial y}\left(\frac{\partial T}{\partial y}\right)+\frac{\partial}{\partial z}\left(\frac{\partial T}{\partial z}\right)\right]\mathrm{d}\Omega\end{aligned} \quad (7)$$

where Ω represents the volume of the control cell. By Stokes' theorem

$$\frac{\partial}{\partial t}\int_{\Omega} T\,\mathrm{d}\Omega = \int_{\Sigma} \frac{k_s}{\rho_s C_s}\left(\frac{\partial T}{\partial x}\mathrm{d}x + \frac{\partial T}{\partial y}\mathrm{d}y + \frac{\partial T}{\partial z}\mathrm{d}z\right) \tag{8}$$

where Σ represents the total area of the control cell.

Assuming that thermal properties of the solid (k_s, C_s, ρ_s) are isotropic and homogeneous, Eq. (8) becomes

$$\int_{\Sigma} \frac{k_s}{\rho_s C_s}\left(\frac{\partial T}{\partial x}\mathrm{d}x + \frac{\partial T}{\partial y}\mathrm{d}y + \frac{\partial T}{\partial z}\mathrm{d}z\right) =$$

$$\frac{k_s}{\rho_s C_s}\sum_{i=1}^{6}(\nabla T_{\text{face}} \cdot \boldsymbol{n}S_i) = \frac{k_s}{\rho_s C_s}\sum_{i=1}^{6}(\nabla T_{\text{face}}) \cdot (\boldsymbol{n}S_i) \tag{9}$$

where $\boldsymbol{n}$ is the unit normal vector on control surface i, ∇T_{face} the gradient of the temperature on each surface and obtained from

$$\nabla T_{\text{face}} = \frac{1}{\Omega_{I+1/2,J,K}}\int_{\sum I+1/2,K} T_{\text{cell}} \cdot \boldsymbol{n}\mathrm{d}S = \frac{1}{\Omega_{I+1/2,J,K}}\sum_{i=1}^{6} T_{\text{cell}} \cdot \boldsymbol{n}S_i \tag{10}$$

with $\Omega_{I+1/2,J,K}$ the volume of the virtual cell. From Eqs. (8)—(10), we obtain

$$\frac{\partial}{\partial t}\int_{\Omega} T\,\mathrm{d}\Omega = \frac{k_s}{\rho_s C_s}\sum_{i=1}^{6}\left(\frac{1}{\Omega_{I+1/2,J,K}}\sum_{i=1}^{6} T_{\text{cell}} \cdot \boldsymbol{n}S_i\right) \cdot (\boldsymbol{n}S_i) \tag{11}$$

which subsequently reduces to the form

$$\frac{\partial T}{\partial t} = \frac{1}{\Omega}\frac{k_s}{\rho_s C_s}\sum_{i=1}^{6}\left(\frac{1}{\Omega_{I+1/2,J,K}}\sum_{i=1}^{6} T_{\text{cell}} \cdot \boldsymbol{n}S_i\right) \cdot (\boldsymbol{n}S_i) \tag{12}$$

The surface heat flux distribution is acquired by the flow field solver. The additional source term method is applied to define the heat flux as an equivalent source term for the control cell.

The method of determining the local time step in the heat conduction computation is the same as the synchronization method and will be introduced below.

1.3 Coupling procedure

With reference to the diagram (Fig. 1), the computation procedure for both loosely and tightly coupled methods is summarized as follows.

(1) The computation is divided into several periods (coupling time steps). To initialize the coupled computations, a steady-state fluid computation is performed at t_1.

(2) Assuming the flow field is "frozen", the structural temperature field steps from t_1 (initial temperature field) to t_2 with the "frozen" rate of heating, as well as the interface temperature at t_2 can be acquired using the thermal conduction solver.

(3) Assuming the structural temperature field is then "frozen", the flow field steps from t_1 to t_2 with the "frozen" interface temperature, and the rate of heating at t_2 is determined using the steady flow field solver.

(4) The final temperature field can be acquired through several iterations between the flow field solver and thermal conduction solver until reaching the final time point (t_n).

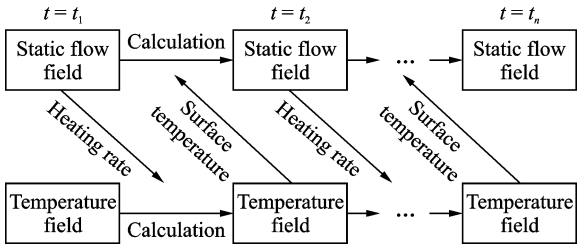

Fig. 1 Procedure for traditional coupling methods

2 Synchronization Method

The traditional coupled methods need to exchange the information of flow field and structural temperature field at the interface, and when one field is being computed, the other is usually kept "frozen". Moreover, a suitable coupling time step is required. Thus, a synchronization method is proposed to overcome these drawbacks and also to satisfy engineering requirements in precision.

2.1 Governing equations and discretization

For the fluid component, the discretization method is the same with the flow field solver in the traditional coupling method. For an ideal gas

$$\rho_f E_f = \frac{p}{\gamma - 1} + \frac{1}{2}\rho_f(u^2 + v^2 + w^2) \tag{13}$$

For the solid component, $u = v = w = 0$. Hence, the first three scalar equations in Eq. (1) are naturally satisfied. The fourth equation in Eq. (1) determines the energy

$$\rho_s E_s = \rho_s C_s T_s \tag{14}$$

The discretization method for the heat equations is the same with Eqs. (6)—(12). In the following section, the determination of local time steps and treatments of the boundary will be presented.

2.2 Determination of the local time steps

Jameson's dual time stepping method is used for temporal discretization, and the implicit LU-SGS scheme is applied to time stepping in the pseudo-iteration. Local time steps for the fluid can be determined using

$$\Delta t_I = \sigma \frac{\Omega_I}{(\hat{\Lambda}_c^I + \hat{\Lambda}_c^J + \hat{\Lambda}_c^K)_I + 4\ (\hat{\Lambda}_v^I + \hat{\Lambda}_v^J + \hat{\Lambda}_v^K)_I} \tag{15}$$

where $\hat{\Lambda}_c^I$ and $\hat{\Lambda}_v^I$ represent spectral radii of the convective flux and the viscous flux in the I-th direction, respectively, defined as

$$\hat{\Lambda}_c^I = (|V^I| + c)\,\Delta S^I \tag{16}$$

$$\hat{\Lambda}_v^I = \max\left(\frac{4}{3\rho_f}, \frac{\gamma}{\rho_f}\right)\left(\frac{\mu_L}{P_L} + \frac{\mu_T}{P_T}\right)\frac{(\Delta S^I)^2}{\Omega_I} \tag{17}$$

where P_L and P_T represent laminar and turbulent Prandtl numbers, respectively; c represents the local speed of sound. The fluid heat conductivity is given by

$$k_f = \frac{\gamma R \cdot \mu_L}{P_L(\gamma - 1)} + \frac{\gamma R \cdot \mu_T}{P_T(\gamma - 1)} = C_p \cdot \left(\frac{\mu_L}{P_L} + \frac{\mu_T}{P_T}\right) \tag{18}$$

or equivalently

$$\frac{\mu_L}{P_L} + \frac{\mu_T}{P_T} = \frac{k_f}{C_p} \tag{19}$$

Like the diffuse viscous equation, the thermal conduction equation is parabolic. Accordingly, the local time step for this equation resembles that for the diffuse viscous equation. Since $\hat{\Lambda}_c^I$ is regarded as 0 in the solid component, the local time steps of the thermal conduction is

$$\Delta t_{I,s} = \sigma \frac{\Omega_I}{4\ (\hat{\Lambda}_{v,s}^I + \hat{\Lambda}_{v,s}^J + \hat{\Lambda}_{v,s}^K)_I} \tag{20}$$

According to the definition ofthe spectral radii of viscous flux for the fluid, and from Eq. (19), the spectral radii of thermal conduction is acquired from

$$\hat{\Lambda}_{v,s}^I = \frac{k_s}{\rho_s C_s}\frac{(\Delta S^I)^2}{\Omega_I} \tag{21}$$

The method of introducing the thermal conduction spectral radii to determine the local time steps is equivalent to the definition of "viscous" in the heat conduction. This ensures that the fluid thermal conduction is consistent with the solid thermal conduction during each pseudo-iteration process. Additionally, there is no need to determine the coupling time step or to freeze the field for either flow or structural temperature.

2.3 Initial and boundary conditions

The static initial flow field and temperature field at $t = 0$ s are required before the synchronous computation. The boundary in the far field is treated using the same condition in loosely/tightly coupled methods. In the following section, the implementation of the boundary conditions between fluid and solid will be presented. The initial coefficient of viscosity of the interface can be determined by the surface temperature and the Sutherland formula, and then the thermal conductivity coefficient k_w of the initial surface can be obtained.

Because of differences in physical properties (such as thermal conductivity and coefficient of viscosity) between fluid and solid, an expanded virtual boundary is introduced to compute the viscous flux of the interface. "Expanded" means that the virtual cells and real cells have same physical properties. Specifically, as sketched in Fig. 2, the cell marked $K = 0$ represents the expanded virtual cell, which has the same properties as the cell $K = 1$. These cells are not real interface cells, but presented for the computation of the boundary derivatives and called expanded virtual cells. These are used to compute the viscous flux, viscous coefficient, and thermal conductivity. Nevertheless, the temperature of interface should be determined by the real cells of the fluid and solid. The temperature of the expanded virtual cell for the fluid is obtained by interpolation

$$T_0 = 2 \times T_w - T_1 \tag{22}$$

where T_0, T_1 represent the temperature of cells $K = 0, 1$, respectively, and T_w denotes the temperature of the interface. It can be obtained by pseudo-time stepping using the continuity of heat flux at the interface[12]

$$k_f \frac{T_f - T_w}{d_f} = k_s \frac{T_w - T_s}{d_s} \tag{23}$$

where d_f and d_s denote the distances between the center of the first layer and the interface in the fluid and solid, respectively; T_f and T_s the temperature in the first layer of the fluid and solid; k_s and k_f the heat conductivities of solid and fluid parts, respectively, determined by the interface temperature. The pressure gradient normal to the wall and the velocity at the wall are zero. The interface density can be obtained using the ideal gas equation.

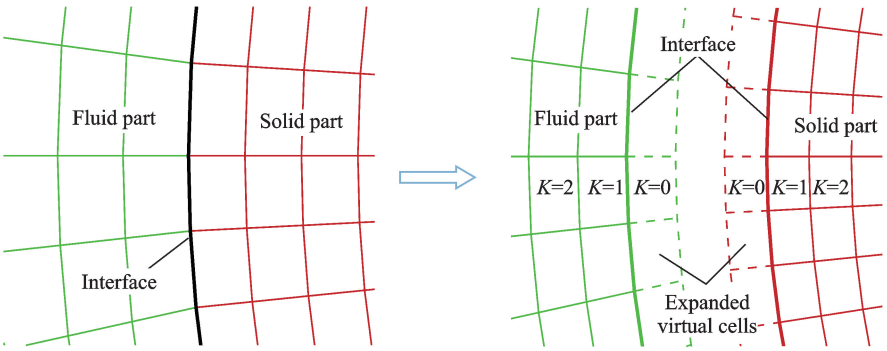

Fig. 2 Expanded virtual boundary

At the interface, the coefficients for heat conductivity and viscous are considered as functions of temperature. Consequently, the implementation of the boundary treatments combines the computation of the flow field and the temperature field more tightly.

3 Applications

Loosely/tightly coupled methods and the synchronization method are assessed by simulating Mach-6.47 flow over a two-dimensional cylinder and Mach-9.86 flow over a three-dimensional biconical surface. The resultant flow behaviors are calibrated using experimental data. All the computations are performed on multiblock structured grids. All lengths are in meters unless otherwise stated.

3.1 Mach-6.47 flow over a two-dimensional cylinder

Similar to Ref. [13], the test model consists of a 12.7-mm-thick, 76.2-mm-diameter, and 321 stainless steel cylinder. Details of the experimental configurations, the tunnel flow conditions, and the experimental results were also given in Ref. [13]. The setting for the thermal properties of the solid and the aerodynamic parameters applied in this section are

$Ma_\infty = 6.47$, $\alpha = 0°$, $T_\infty = 241.5$ K, $T_w = 294.4$ K

$\rho_\infty = 1.012 \times 10^{-2}$ kg/m^3, $p_\infty = 7.018 \times 10^2$ Pa

$\rho_s = 9030$ kg/m^3, $k_s = 16$ W/(m·K)

$C_s = 500$ J/(kg·k)

The grids representing the flow domain and the cylinder (Fig. 3) consist of 12 000 cells in the flow domain and 3 000 cells in the cylinder with the same discretization along the interface. Following Ref. [14], the smallest cell in the flow domain is only 0.010 16 mm in the direction normal to the cylinder surface. A detailed study of this model was presented in Ref. [14], and it has been used to validate algorithms by many researchers. In this paper, the numerical results are also compared with those in Ref. [14].

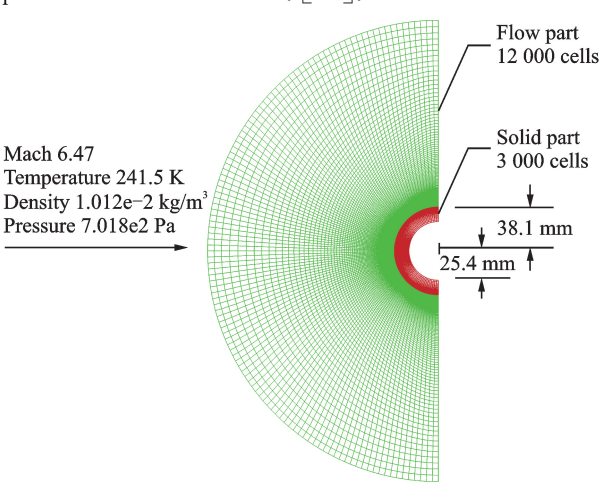

Fig. 3 Fluid-solid finite volume model for flow over a 76.2-mm-diameter cylinder

The major difficulty in the fluid analysis is the prediction of the rates of aerodynamic heating, because a very accurate resolution of the flow temperature gradient normal to the cylinder surface is required. Both the synchronization method and loosely/tightly coupled methods need a static initial flow field at $t=0$ s before computations. The computed flow temperature distribution at $t=0$ s (Fig. 4) along the flow symmetry line ($y=0$) clearly illustrates the sharp gradients that must be resolved. The free-stream temperature increases sharply from 241.5 K to about 2 200 K across the bow shock. Within a very thin layer at the flow stagnation point, the temperature drops sharply from 2 200 K to a surface temperature of 294.4 K. Thus, these computation results are in good agreement with Ref. [14]. Comparison of the density contours with those of Ref. [14] (Fig. 5) shows that the shock wave is well captured.

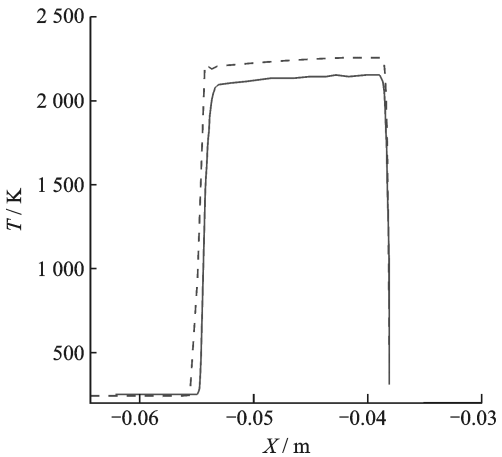

Fig. 4 Comparison of fluid temperature distributions between the reference and present model taken along the centerline of the initial flow

And then, we can continue the computation of coupled methods and synchronization method. For loosely coupled methods, the flow field and the structural temperature field are updated every 0.2 s. Physical time step of tightly coupled methods should be consistent with the synchronization method, determined by a trial computation of stagnation temperature at $t=2.5e-3$ s with different physical time steps. The results are obtained by synchronization method with 100 pseudo-iterations (Table 1).

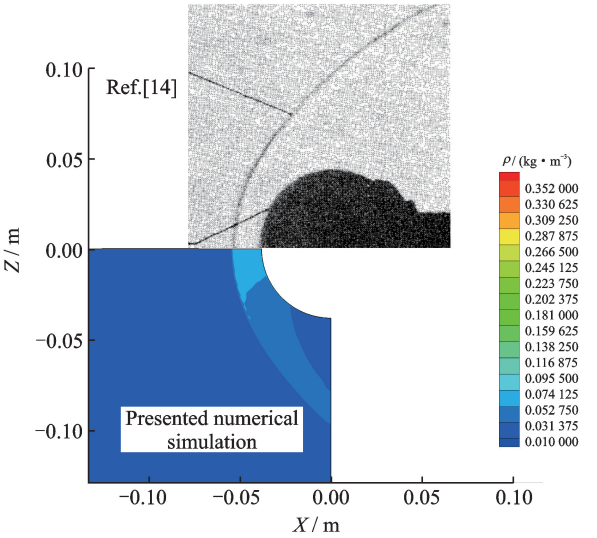

Fig. 5 Comparison of density contours between reference and present model for Mach-6.47 flow over a 3-in-diameter cylinder

Table 1 Stagnation temperature at $t=2.5e-3$ s with different physical time steps

Physical time step/s	2.5e−3	1.25e−3	6.25e−4	3.125e−4
Stagnation temperature/K	296.783	297.208	297.466	297.584

Comparisons of the temperature contours at $t=2$ s among the reference, the loosely/tightly coupled methods, and the synchronization method are shown in Fig. 6, in which temperature values are cell centered. Since the dimension of temperature in Ref. [14] is given using the Rankine scale, the temperature has been converted to enable a clear comparison of contours. For the loose-

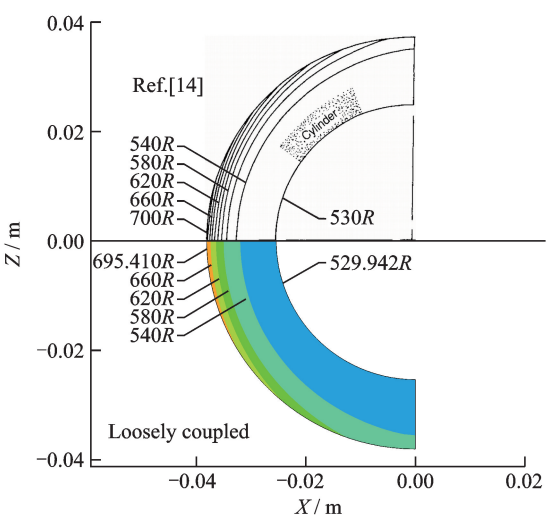

(a) Loosely coupled method

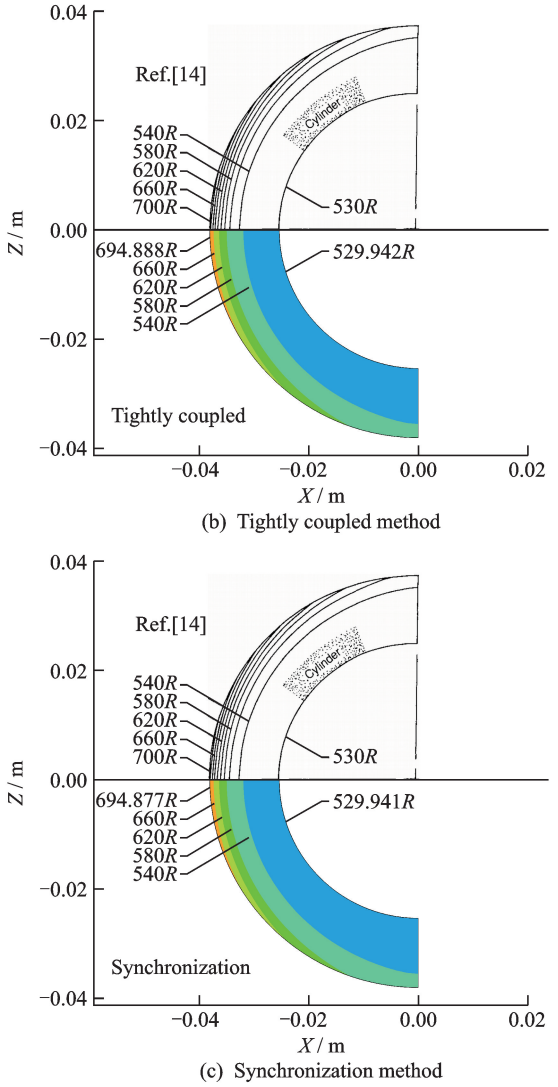

Fig. 6 Comparisons of predicted temperature contours at $t=2$ s of the loosely coupled method, the tightly coupled method and the synchronization method with the result in Ref. [14]

ly coupled method, the stagnation temperature is 386.339 K (695.410 R) at $t=2$ s; For the tightly coupled method, the stagnation temperature is 386.049 K (694.888 R) at $t=2$ s; For the synchronization method, the stagnation temperature is 386.043 K (694.877 R) at $t=2$ s; In Ref. [14], the stagnation temperature is 388.889 K (about 700 R) at $t=2$ s. Obviously, the results of three methods are in good agreement with those from the experiment.

Comparisons of time histories of the stagnation heat flux between the experiment, the loosely/tightly coupled methods, and the synchronization method [Fig. 7(a)] show that the stagnation heat flux drops sharply during the early period of the computation, but the trend gradually slows down in the time remaining. Due to the influence of heat flux, the time histories of stagnation temperature of these methods increase in the similar trend [Fig. 7(b)].

In this case, the model is continuously heated by hypersonic flow, the stagnation temperatures with these three methods are all found to be in good agreement with experiment. The temperature contours, stagnation temperatures and heat fluxes of the three methods are almost same. Therefore, it is acceptable to apply the either the loosely/tightly coupled methods or the synchronization method to aerothermal analysis of continuously heated problem in engineering.

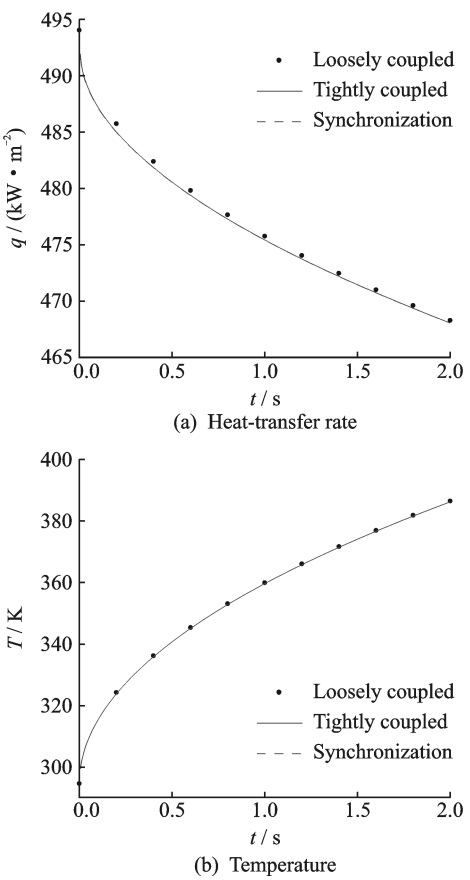

Fig. 7 Comparisons of heat-transfer rates and temperatures at stagnation between loosely coupled method, tightly coupled method, and synchronization method

3.2 Mach-9.86 flow over a three-dimensional bicone

The model (Fig. 8) used in the experiment

was fabricated from stainless steel except for the nose tip, which was made from MACOR machinable glass-ceramic. For the convenience, the model presented here is uniquely machined from the MACOR. In accounting for the variation with temperature, the thermal properties of MACOR, taken from Ref. [15], are as follows.

For 300 K$<T<$400 K

$$k_s = 1.614 \text{ W/m} \cdot \text{K}$$

For 295 K$<T<$673 K

$$C_s = 193.53 + 3.348\,13 \times T - 1.001\,61 \times 10^{-2} \times T^2 + 2.811\,25 \times 10^{-5} \times T^3 - 4.248\,05 \times 10^{-8} \times T^4 + 2.334\,33 \times 10^{-11} \times T^5 \text{ J/(kg} \cdot \text{K)}$$

For 298 K$<T<$773 K

$$\rho_s = 2\,543.84 - 8.0 \times 10 - 2T \text{ kg/m}^3$$

The grids representing the flow domain and the bicone (Fig. 9) consist of 1 436 974 cells in the flow domain and 1 048 174 cells in the bicone with the same discretization along the interface. The height of the first layer is determined from the grid Reynolds number[16]

$$Re_c = \frac{\rho_\infty v_\infty n}{\mu_\infty} \tag{24}$$

where the feature size n is usually taken as the normal height of the first layer of mesh near the wall. In accordance with Ref. [16], the smallest cell in the flow domain is 0.107 mm in the direction normal to the surface of stagnation. Details of the experimental configurations, the tunnel flow conditions, and the experimental results are given in Ref. [17]. The aerodynamic parameters applied in this section are

$$Ma_\infty = 9.86,\ \alpha = 0°,\ T_\infty = 48.88 \text{ K},\ T_w = 300 \text{ K}$$

$$\rho_\infty = 4.271 \times 10^{-3} \text{ kg/m}^3,\ p_\infty = 5.992 \times 10 \text{ Pa}$$

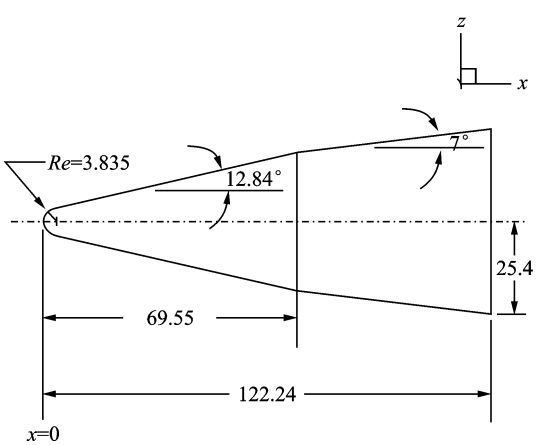

Fig. 8 Details of the profile of the model (mm)

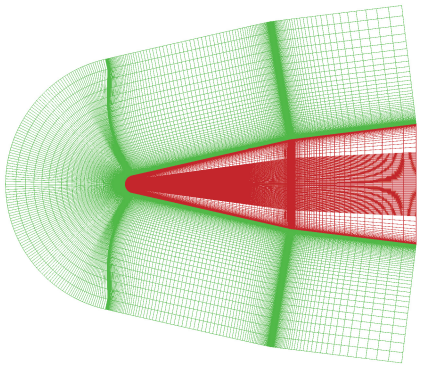

Fig. 9 Symmetry plane for flow domain and bicone

As mentioned in Ref. [17], in the experiment, $t=0$ s is defined as the initiating time when the surface temperature of the model begins to increase as it is inserted into the flow from a sheltered position. According to the time history of heat flux, the time interval can be divided into two stages. During the first 0.35 s, the flow field is not stable, and the model can be considered as be accelerating in this sub-interval; the heat flux reaches a maximum at $t=0.35$ s and begins decreasing slowly after the peak point. Assuming that the density and pressure of the free-stream remain constant, the velocity is considered to increase with time to simulate the accelerating period. Kang et al.[18] applied the Kemp-Riddell corrected formula

$$q_{wst} = \frac{110\,311.7}{\sqrt{R_N}} \left(\frac{\rho_\infty}{\rho_0}\right) \frac{1}{2} \left(\frac{V_\infty}{V_c}\right) 3.15 \left(\frac{h_{st} - h_w}{h_{st} - h_{300\text{ K}}}\right) \tag{25}$$

From the time history of the heat flux for the reference, and assuming that the wall temperature is a constant (300 K) during the accelerating period, the Mach number during the interval $t=0$ s to $t=0.35$ s can be obtained from Eq. (25), which is displayed Table 2.

Table 2 Variation of Mach number from $t=0$ s to $t=0.35$ s

t/s	q/(kW · m^{-2})	Velocity of free stream/(m · s^{-1})	Ma
0	—	51.86	0.37
0.1	10	417.7	2.98
0.2	100	867.5	6.19
0.3	300	1229	8.77
0.35	373	1382	9.86

For the loosely coupled method, the flow field and the structural temperature field are updated every 0.1 s. For both the tightly coupled method and the synchronization method, the flow field and the structural temperature field are updated every 0.001 s with 400 steps pseudo-iteration. Actually, the experimental environment is more complex than that assumed in the numerical simulation because keeping the density and pressure of the free-stream constant is difficult. The difference between the numerical methods and experiment is attributed to free-stream turbulence in the test stream, which is not taken into account by the numerical method. Moreover, the whole computation concludes subsonic flow, transonic flow, supersonic flow, and hypersonic flow. The height of the first layer and the far field of the grid are designed for hypersonic flow, resulting in computation errors during the subsonic and transonic periods. Furthermore, differences between the assumption (a constant wall temperature of 300 K during the accelerating period) and the experiment may influence the evaluation of the Mach number for the free stream using Eq. (26). Additionally, apart from the MACOR nose tip, the model is fabricated from stainless steel. Obviously, as noted in Ref. [17], the entire model ideally should be made of MACOR glass-ceramic, but for this experiment it is not structurally or economically feasible.

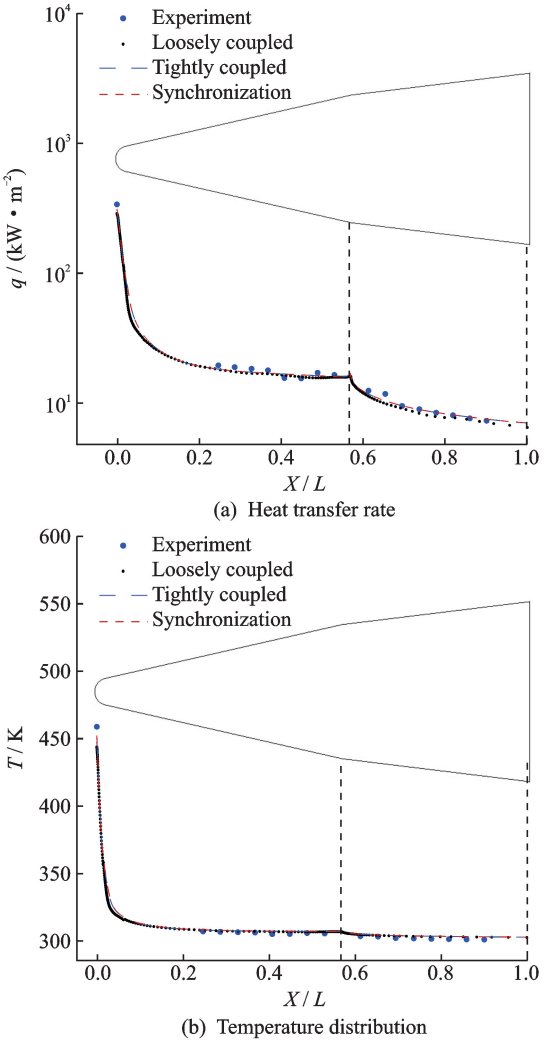

Fig. 10 Comparisons of the longitudinal heat transfer rates and temperature distributions at $t=1.0$ s between the experiment, the loosely coupled method, the tightly coupled method, and the synchronization method

Comparisons of the longitudinal heat transfer rate and temperature distribution at $t=1.0$ s among the experiment, the loosely/tightly coupled methods, and the synchronization method (Fig. 10) show that the heat fluxes and temperatures obtained by all these numerical methods are basically the same in the non-stagnation region. The synchronization method performs better than the other methods in calculation of stagnation heat flux and temperature.

Comparisons of temperature contours in solid domain at $t=0.35$ s between the loosely coupled method, the tightly coupled method, and the synchronization method (Fig. 11) show that the temperatures obtained by the synchronization method and the tightly coupled method, which are basically the same, are slight higher than those obtained by the loosely coupled method. That is why the surface heat fluxes obtained by the loosely coupled method are slight higher than those obtained by the other two methods at $t=0.35$ s (Fig. 12). Because of the increment of temperature, the surface heat flux at $t=1.5$ s reduces evidently compared with that at $t=0.35$ s as shown in Fig. 12.

Time-history comparisons of the heat flux at stagnation among the experiment, the loosely/tightly coupled methods, and the synchronization method (Fig. 13(a)) show that the heat fluxes

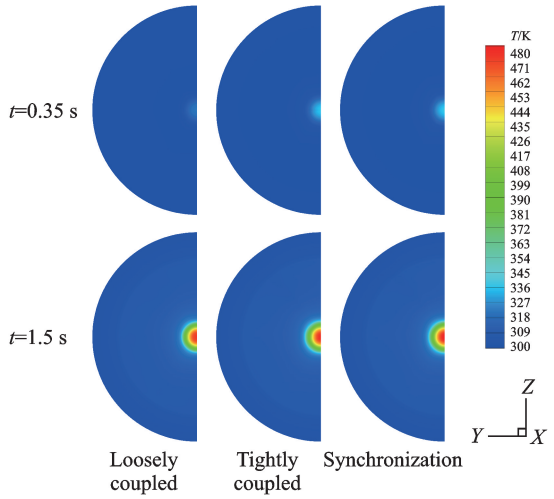

Fig. 11 Comparisons of temperature contours in solid domain at $t=0.35$ s and $t=1.5$ s between the loosely coupled method, the tightly coupled method, and the synchronization method

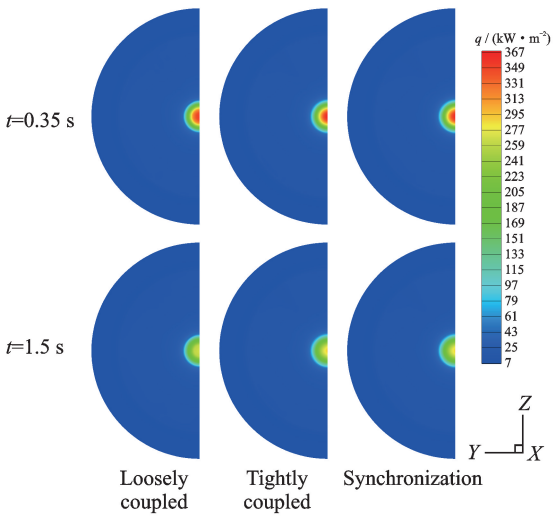

Fig. 12 Comparisons of surface heat flux contours at $t=0.35$ s and $t=1.5$ s between the loosely coupled method, the tightly coupled method, and the synchronization method

obtained by the synchronization method and the tightly coupled method, which are basically the same, are closer to the experimental data than those obtained by the loosely coupled method. As reported in Ref. [17], the measured results for the temperature at stagnation are 402.3 K, 461.1 K, and 493.8 K at $t=0.5$ s, $t=1.0$ s, and $t=1.5$ s, respectively. Similar comparisons for the temperature at stagnation (Fig. 13(b)) show that the final stagnation temperatures at $t=1.5$ s, computed by the loosely/tightly coupled methods, and the synchronization method are 482.08 K, 486.30 K, and 490.58 K, respectively. The stagnation temperature increases sharply from 300 K to about 500 K in 1.5 s. Similarly, the whole aerodynamic heating is composed of two stages: (1) The free-stream varies during $t=0$ s to $t=0.35$ s, and the heat flux grows sharply to a maximum at $t=0.35$ s (unsteady flow); (2) from $t=0.35$ s to $t=1.5$ s, the rate of aerodynamic heating decreases slowly (continuous heating flow).

During the first stage, the Mach number increases from 0.37 to 9.86, and the stagnation temperature grows markedly by about 50 K in 0.35 s. Indeed, the stagnation temperature increases slightly during the first 0.2 s. In other words, the rise in stagnation temperature mainly occurs within 0.15 s (from $t=0.2$ s to $t=0.35$ s). The unsteady flow effect of this period is very significant. Hence, the differences between the synchronization method and the loosely coupled method are mainly manifested during this period. The results (Fig. 13(a)) during the accelerating period computed by the tightly coupled method and the synchronization method agree better than those by the loosely coupled method and experiment data in terms of accuracy. This is mainly caused by the unsteady flow field during this time period.

During the second stage, the model is continuously heated by hypersonic flow, similar to the two dimensional case mentioned above. At the beginning of the second stage, there still exists unsteady effect in flow field, resulting in the difference of stagnation temperature between the tightly coupled method and the synchronization method. The stagnation temperature of the synchronization method matches the experiment data better than that of the tightly coupled method during this period in terms of the accuracy. In the following computation, the trends of heat flux and temperature of these three methods are almost same.

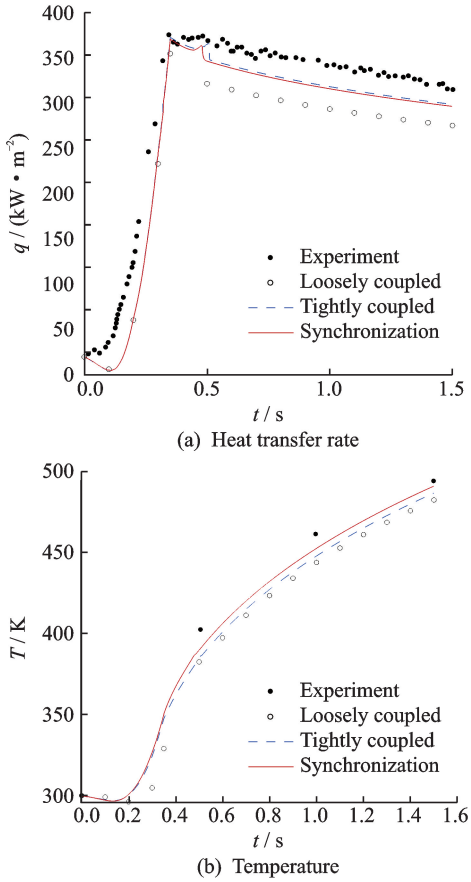

Fig. 13 Time history comparisons of heat transfer rates and temperatures at stagnation between the experiment, the loosely coupled method, the tightly coupled method, and the synchronization method

4 Conclusions

In this paper, an accurate and efficient synchronization method is developed for fluid-thermal study of hypersonic flows, through which three major conclusions are drawn as follows.

(1) In the developed method, the flow field and the structure temperature field are calculated simultaneously by solving the unified governing equations. As compared with conventional coupled methods, the synchronization method is physically more reasonable since fewer approximations are made. Numerically, without the need to combine different methods for solving the flow field and the structure temperature field, it is easier to be implemented.

(2) In the continuous heating problems, the stagnation temperatures and heat fluxes predicted by all the three methods are in good agreements with the results of the reference. It is acceptable to apply either loosely/tightly coupled methods or the synchronization method to aerothermal analysis of the continuous heating problems in engineering.

(3) In the unsteady flow-thermal hypersonic flows, the stagnation heat fluxes obtained from the synchronization method and the tightly coupled method are closer to the experimental data than those obtained from the loosely coupled method. Further, the stagnation temperature obtained from the synchronization method is closer to the experimental data than that obtained from the tightly coupled method. Thus, the presented synchronization method is a more accurate method for the unsteady hypersonic flow-thermal computations.

Acknowledgements

This work was supported by the National Natural Science Foundation of China (No. 11872212). All numerical simulations have been conducted on the computers of Aerodynamic Department of College of Aerospace Engineering at Nanjing University of Aeronautics and Astronautics. The authors also gratefully acknowledge the technical insights of associate professor Wu Jie of Aerodynamic Department of College of Aerospace Engineering at Nanjing University of Aeronautics and Astronautics.

References:

[1] KAZEMI-KAMYAB V, VON ZUIJLEN A H, BIJL H. Analysis and application of high order implicit Runge-Kutta schemes for unsteady conjugate heat transfer: A strongly-coupled approach[J]. Journal of Computational Physics, 2014, 272(9): 471-486.

[2] XIA G, LIU X J, CHENG W K, et al. Numerical simulation of coupled aeroheating and solid heat penetration for a hypersonic blunt body[J]. Journal of National University of Defense Technology, 2003, 25(1): 35-39. (in Chinese)

[3] CLEMENTE M D, RUFOLO G, IANIRO A, et al. Hypersonic test analysis by means of aerothermal coupling methodology and infrared thermography[J]. AIAA Journal, 2013, 51(7):1755-1769.

[4] SONDAK D L, DORNEY D J. Simulation of coupled unsteady flow and heat conduction in turbine stage[J]. Journal of Propulsion and Power, 2000, 16

(6):1141-1148.

[5] HAUPT M, NIESNER R, UNGER R, et al. Computational aero-structural coupling for hypersonic applications[C]//AIAA/ASME Joint Thermophysics and Heat Transfer Conference. San Francisco, USA: AIAA, 2006.

[6] ZHANG S, CHEN F, LIU H. Integrated fluid-thermal-structural analysis for predicting aerothermal environment of hypersonic vehicles[C]//52nd Aerospace Sciences Meeting. National Harbor, USA: AIAA, 2014.

[7] CROWELL A R, MILLER B A, MCNAMARA J J. Computational modeling for conjugate heat transfer of shock-surface interactions on compliant skin panelss[C]//52nd AIAA/ASME/ASCE/AHS/ASC Structures, Structural Dynamics and Materials Conference. Denver, USA: AIAA, 2011.

[8] GUO S, XU J, QIN Q, et al. Fluid-thermal interaction investigation of spiked blunt bodies at hypersonic flight condition[J]. Journal of Spacecraft & Rockets, 2016, 53(4): 629-643.

[9] VEERARAGAVAN A, BERI J, GOLLAN R J. Use of the method of manufactured solutions for the verification of conjugate heat transfer solvers[J]. Journal of Computational Physics, 2016, 307: 308-320.

[10] GENG X, ZHANG H, SHEN Q, et al. Study on an integrated algorithm for the flow fields of high speed vehicles and the heat transfer in solid structures[J]. Acta Aerodynamica Sinica, 2002, 20(4): 422-427.

[11] DUCHAINE F, CORPRON A, PONS L, et al. Development and assessment of a coupled strategy for conjugate heat transfer with large eddy simulation: Application to a cooled turbine blade[J]. International Journal of Heat and Fluid Flow, 2009, 30(6): 1129-1141.

[12] TAO W. Numerical Heat Transfer[M]. 2nd ed. Xi'an: Xi'an Jiaotong University, 2001. (in Chinese)

[13] WIETING A R, HOLDEN M S. Experimental study of shock wave interference heating on a cylindrical leading edge at Mach 6 and 8[C]//22nd Thermophysics Conference. Honolulu, USA: AIAA, 1987.

[14] DECHAUMPHAI P, WIETING A R, THORNTON E A. Flow-thermal-structural study of aerodynamically heated leading edges[J]. Journal of Spacecraft & Rockets, 1989, 26(4): 201-209.

[15] MILLER C G Ⅲ. Comparison of thin-film resistance heat-transfer gages with thin-skin transient calorimeter gages in conventional hypersonic wind tunnels: NASA Technical Memorandum 83197 [R]. USA: NASA, 1981.

[16] YAN C, YU J, LI J. Scheme effect and grid dependency in cfd computations of heat transfer[J]. Acta Aerodynamica Sinica, 2006, 26(1): 125-130.

[17] MILLER C G Ⅲ. Experimental and predicted heating distributions for biconics at incidence in air at Mach 10: NASA Technical Paper 2334 [R]. USA: NASA, 1985.

[18] KANG H, YAN C, LI T, et al. Numerical study of aeroheating predictions for hypersonic reentry bodies [J]. Journal of Beijing University of Aeronautics and Astronautics, 2006, 32(12): 1395-1398. (in Chinese)

Mr. **Shen Ennan** received B. E degree in aircraft design and engineering in 2008 and M A. Eng degree in aeronautical engineering in 2015 from Nanjing University of Aeronautics and Astronautics (NUAA), where he continues to study for Ph. D of Fluid Mechanics. His research is focused on computational fluid dynamics, hypersonic aero-thermal coupling computation, aero-elasticity and relevant fields.

Prof. **Lu Zhiliang** received B. S. and Ph. D. degrees in aerodynamics from Nanjing University of Aeronautics and Astronautics (NUAA) in 1984 and 1997, respectively. In 1995, he joined the Deutsches Zentrum fur Luft-und Raumfahrt for cooperative research. He has been working as a professor of aerodynamics of NUAA since April 2001. His research is focused on computational fluid dynamics, aero-elasticity and relevant fields.

Mr. **Zhou Di** received B. E degree in aircraft design and engineering in 2008 from Nanjing University of Aeronautics and Astronautics (NUAA), where he continues to study for Ph. D of Fluid Mechanics. His research is focused on computational fluid dynamics, turbo-machinery aero-elasticity and relevant fields.

Dr. **Guo Tongqing** received Ph. D degree in aerodynamics from Nanjing University of Aeronautics and Astronautics (NUAA) in 2006. In 2016, he worked as a visiting scholar in the National University of Singapore. His research is focused on computational fluid dynamics and CFD/CSD coupling numerical computation.

(Production Editor: Zhang Bei)